Neural representations of harmonic function in musical imagery

Tudor Popescu[1,2~*], Nicolas Farrugia[3~], Hannes Ruge[4], Oren Boneh[5], Fernando Bravo[6,7], Xing Tian[8-10], Martin Rohrmeier[11]

[1] Department of General Psychology, University of Padova, 35131, Padova, Italy
[2] Vienna Cognitive Science Hub, University of Vienna, 1090 Vienna, Austria
[3] IMT Atlantique, Research Laboratory in Information and Communication Science and Technology (Lab-STICC), UMR CNRS 6285, Brest, France
[4] Department of Psychology, TU Dresden, 01159 Dresden, Germany
[5] Department of Music, University of California Berkeley, CA 94720 Berkeley, US
[6] Department of Clinical Neuroscience, University of Cambridge, CB2 3EB Cambridge, UK
[7] Music Technology and Computational Neuroscience, Cognition and Consciousness Imaging Group, University of CB2 3EB Cambridge, UK
[8] Division of Arts and Sciences, New York University Shanghai, 200122 Shanghai, China
[9] Shanghai Key Laboratory of Brain Functional Genomics (Ministry of Education), School of Psychology and Cognitive Science, East China Normal University, 200050 Shanghai, China
[10] NYU-ECNU Institute of Brain and Cognitive Science at NYU Shanghai, 200122 Shanghai, China
[11] Digital and Cognitive Musicology Lab, Digital Humanities Institute, École Polytechnique Fédérale de Lausanne (EPFL), 1015 Lausanne, Switzerland
[~] shared first-authorship
[*] to whom correspondence should be addressed: tudor.popescu@oxon.org

Please note: This paper is currently undergoing peer-review. We welcome questions, comments, and constructive criticism for the current preprint, bearing in mind that it is a draft subject to revision.

Abstract

Relations among chords ("harmonic syntax") lie at the heart of music listening. Notably, harmonic function, a chord's standing within a key, modulates expectations emerging as a piece unfolds. But how are such relations parsed when music is merely heard in our minds, i.e. during musical imagery? We used fMRI to uncover neural signatures underlying the internal generation of (audible or silenced) musical phrase closures, in an "active listening" paradigm. In different chord sequences, harmonic contexts established strong expectations for target chords that fulfilled either tonic or dominant harmonic functions, within a given musical key. Controlling for acoustic content, classifiers decoded the key of the chord sequence in both Perception and Imagery conditions; the key matched the target's harmonic function. Representational Similarity Analysis further suggested "key" was saliently encoded, which supports an interpretation of the chord sequence being processed holistically, i.e., in its full harmonic context. We propose harmonic function as the manifestation of a generative model transforming acoustic representations into abstracted representations along the imagery–perception continuum, governed by key as a long-distance harmonic property. Framed this way, our results address the previously unanswered theoretical question of how harmonic expectation affords mental representations usable to inwardly or outwardly generate music.

Keywords

musical imagery, harmonic syntax, tonality, musical key, predictive coding, supplementary motor area, fMRI

1. INTRODUCTION

Music is a cherished mental experience, whether heard or merely imagined. Repeated exposure to music leads to implicit acquisition of mental representations of pitch, melody, key, harmony, timbre, rhythm, metre, and other musical features (Rohrmeier & Rebuschat, 2012; Tillmann, 2005). These representations may afford expectations unfolding at multiple levels and time-scales, extending, in the tonal realm, from note-to-note regularities to the harmonic structure of entire pieces (Huron, 2006; Rohrmeier, 2013; Schaefer, 2014). Such expectations are generated by the underlying system of tonality (Hyer, 2001; Vuust et al., 2022).

A major source of tonal expectations is harmonic syntax, the set of rules characterising relations between chords in a given tonal musical culture (Rohrmeier, 2020; Steedman, 1984; also see Gauldin, 2000). A central aspect of Western tonal harmony is **harmonic function**, which describes the role that a particular chord plays in the context of a harmonic progression, itself characterised by a musical **key**. In chord sequences, composers control tonal expectations – at chord, phrase and piece level – and, in turn, tonal tension (Farbood, 2012; Lerdahl & Krumhansl, 2007). This permits music to be "predictably surprising" (Koelsch et al., 2019; Rohrmeier & Koelsch, 2012).

Predictive mechanisms enable not just comprehending music we hear, but also evoking music in our mind's ear. **Musical imagery (MI)** can arise involuntarily (Farrugia et al., 2015; Liikkanen & Jakubowski, 2020). However, used to actively generate music "on demand" (Huovinen & Tuuri, 2019), it is an ability central to musicianship (Gordon, 1984). Forming predictions about a musical event involves a mental model of how we might ourselves generate it (Koelsch et al., 2019), based on articulatory motor commands attempting to generate their auditory consequences (Tian & Poeppel, 2010, 2012). When sufficiently vivid, predictions morph into imagery (Janata, 2001), which in turn updates the predictions (Schaefer, 2014). This generative account of MI is in line with predictive coding accounts of perception (Bastos et al., 2012; Mumford, 1992), and speaks to the cognition–perception–action continuum (Clark, 2013). Hearing and imagining music both afford continuous updating of predictive models aiming to minimise prediction error (Koelsch et al., 2019). In *active inference* (Friston et al., 2011), this can be achieved e.g. by the action of singing along to reinforce the key of a harmonically-ambiguous tune. **Active listening** thus constitutes an ecological paradigm for the study of music (Vuust et al., 2022).

Similar patterns of brain activation exist during auditory imagery as during listening, with critical involvement of belt (Halpern et al., 2004; Halpern & Zatorre, 1999; Herholz et al., 2012; Linke & Cusack, 2015; Schürmann et al., 2002; Zatorre & Halpern, 2005) and possibly primary auditory cortices (Kraemer et al., 2005; Meyer et al., 2010), and their motor projections (Rauschecker, 2011). Activity in this network enabled decoding various features of heard or imagined sound, such as melodic interval (Klein & Zatorre, 2015) and sound category (Linke & Cusack, 2015; Meyer et al., 2010). These findings support proposed notions of a perception–imagery continuum for music (Gracyk, 2019; Janata, 2001).

Generating MI typically involves subvocalisation, minute movements of the larynx that motorically act out internally-represented auditory images (Halpern et al., 2004; Herholz et al., 2012; Lima et al., 2016; Zatorre et al., 1996). Subvocalisation relies on motor and premotor cortices, that activate when humans sing or imagine doing so (Bangert et al., 2006; Halpern et al., 2004; Herholz et al., 2012; Kleber & Zarate, 2014). It should be noted that, while MI can be elicited in paradigms even when subvocalisation is not explicitly encouraged (Regev et al., 2021), involuntary occurrence of this phenomenon remains difficult to ascertain.

Decoding MI for the pitch domain in tonal contexts has recently been demonstrated, using space- and time-resolved brain recordings (May et al., 2022; Sankaran et al., 2018, 2020). Those results speak to the salience of higher-order knowledge of the (diatonic) tonal hierarchy, as applied to note sequences. However, to our knowledge, MI for the harmony domain is novel. Here we present a paradigm to decode abstracted versus veridical representation of MI for chords in tonal context. One important open question remains how harmonic syntax interfaces with the generative process of internally recreating music along the perception–imagery continuum (Schaefer, 2014). Hypothesising this family of mental processes is underlied by a single generative model of tonal music, we investigated the neural representation of harmonic function in it, under both imagery and perception scenarios, by manipulating chord-by-chord expectation in an "active listening" paradigm. We hypothesise, specifically, that harmonic function transforms surface representations into abstracted internal representations that, as in perception, are governed by long-distance harmonic dependencies. Whereas most work to date focused on the melodic or rhythmic aspects of MI, our paradigm examines, for the first time to our knowledge, MI for polyphonic music, by controlling the relevant harmonic building-blocks.

2. MATERIALS & METHODS

2.1. Participants

Thirty-five healthy adults (12 males, 23 females; ages 18-45, 24.4±6.2 years) were recruited as volunteers, and compensated for their time at a rate of 10 EUR/hour. Only data from N=19 participants were available for some of the analyses, due to incomplete questionnaire inputs. Recruitment was done via local adverts, with no particular specification of musical background. Participants declared to have no difficulties in hearing, and gave informed consent to participate.

2.1.1 Ethical approval

This study was approved by the Ethical Committee of the TU Dresden: ethics ref. nr. EK 107032016, application "Neurokognitive Grundlagen der Musikvorstellung" submitted by T.P.

2.2. Stimuli

We employed two forms of canonical musical phrases: authentic cadences and half cadences. Cadences can be thought of as the musical equivalent of punctuation, bringing a phrase to an ending that carries with it varying degrees of closure, also referred to as cadential closure (Rohrmeier & Neuwirth, 2015). Empirical studies confirm that listeners can differentiate among those and other types of cadences (e.g., Sears et al., 2014).

Primary stimuli were eight short tonal chord sequences, each consisting of seven chords: a 6-chord *context* followed by a final *target* chord. Chords sounded 2s each, for a total duration of 14s per stimulus. Stimuli were created using a piano tone sampled from a Steinway Model-C grand piano (http://www.pianosounds.com/) and rendered via MIDI using MuseScore (musescore.org).

For increased control over voice leading, rather than selecting equal-length chord sequences from the extant musical canon, stimuli were expressly composed by a professional composer (O.B.). The aim was to attain a strong feeling of closure leading up to – and attained on – the target chord, which realised either an authentic or a half cadence. That is, the target's harmonic function was either the key's tonic (first scale degree, or **I** in Roman numeral notation) or its dominant (fifth scale degree, **V**), respectively. This was the defining basis for our critical category, based on harmonic function (*HarmonicFn*; see below).

2.2.1 Stimulus versions under the 2×2 categories

Within each harmonic function, target chords in each chord sequence had surface realisations as (i.e., used pitches of) either C-major or F#-major chords, with the same voicing for each, only transposed. See Table 1, the two example stimuli in Figure 1, and the complete scores at osf.io/qu5vy. The 2×2 categories thus defined were *HarmonicFn* (Tonic / Dominant) × *Surface* (C major / F# major). Between different stimuli, target chords matched in terms of one of the categories but differed on the other.

Chord sequences with two different contexts were composed for each combination of categories (rather than merely transpose one context), for a total of eight primary stimuli. A version of each was then rendered as an exemplar in each of three experimental conditions (P, I, C; see below). Having more than one exemplar was necessary to enable the decoding analyses, through classifier training on both exemplars, to dissociate components that arise through structural vs. surface differences between the sounds (Klein & Zatorre, 2015).

By necessity, stimuli employed four different musical keys. For instance, stimuli ending on a dominant target surface-realised as a C-major chord were in the key of F-major (see Table 1). For any given chord sequence, the key was operationalised in terms of its membership in the *HarmonicFn* × *Surface* categories, which defined the resultant (redundant) third category of *Key*. All three categories were used in the analyses.

Table 1: Categorisation scheme for stimuli across the three experimental conditions (**P**erception, **I**magery, **C**ontrol), based on the categories *HarmonicFn* (target chord's harmonic function) and *Surface* (its actual pitches), which together uniquely determine the *Key* of a chord sequence. To illustrate the identity of unique stimuli, exemplars are named based on their *HarmonicFn* and *Surface* membership, exemplar number (two in each case), and condition (preceded by underscore). Two of those stimuli are referred to, by these names, in the caption of Figure 1. Note that *HarmonicFn* does not also prefix names of stimuli in the control condition, since those are isolated chords, with no context, characterised only by their *Surface*.

HarmonicFn category	*Surface* category	*Key* category	Exemplars for **P**erception condition	Exemplars for **I**magery condition	Exemplars for **C**ontrol condition
Tonic	C	C	TC1_P	TC1_I	C_C
			TC2_P	TC2_I	
	F#	F#	TF#1_P	TF#1_I	F#_C
			TF#2_P	TF#2_I	
Dominant	C	F	DC1_P	DC1_I	C_C
			DC2_P	DC2_I	
	F#	B	DF#1_P	DF#1_I	F#_C
			DF#2_P	DF#2_I	
Number of unique stimuli in each condition			8	8	2
Number of unique stimuli across all conditions			18		

2.2.2 Stimulus versions under the 3 conditions

Stimuli for the main task (see Figure 1) were generated under three conditions (**P**erception, **I**magery, and **C**ontrol), defined in terms of which combination of context and target chords were audible. In **P**, all 7 chords were audible, allowing us to train subjects' expectations about the target. In **I**, the context chords were audible while the target chord was silenced. In **C**, stimuli only consisted of the target chord itself, with no context; therefore, only the *Surface* category was definable for **C** stimuli, in single exemplars (as opposed to double, as in **P** and **I**). There were thus a total of 18 unique stimuli used in the experiment (**P** and **I**: 8; **C**: 2; see Table 1).

2.3. Procedure

Each participant underwent a behavioural pre-test (a humming task), which conditioned continuation to the fMRI task. Each of these tasks is described below.

2.3.1 Humming pre-test

Participants first took part in a behavioural pre-test intended to maximise the chance that they would, in the **I** condition, imagine the correct target (silenced, as opposed to the **P** version). The pre-test also aimed to lead participants to the same (subvocalisation-based) active listening strategy for MI in the main task. The task was similar to that used in fMRI (see below), except only three blocks were used (two **I** blocks, one **P**). The participants' hummed outputs were rated in terms of how well they matched the current stimulus' target chord. Namely, a "correct" response was coded if the hummed note was part of the chord. An average percentage correct response rate was computed, and only those participants with >75% scores were progressed to the fMRI stage.

2.3.2 Main task (fMRI)

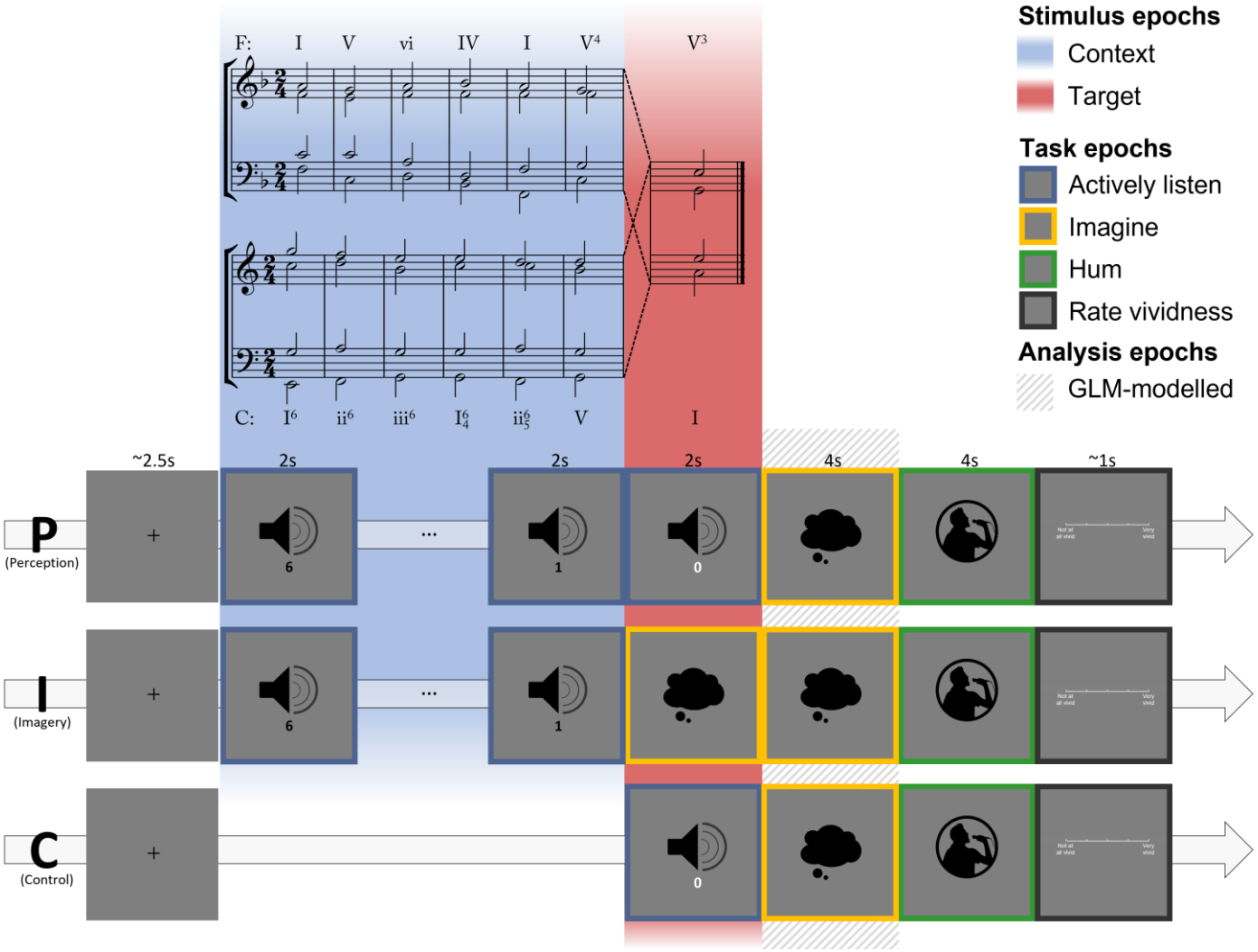

Figure 1: **Task and stimuli**. Top of figure: Stimulus examples with scores, namely exemplars DC1_P, above, and TC1_P, below (see Table 1; for complete stimulus scores and audio files, see online repository at osf.io/qu5vy). Roman numerals denote a chord's harmonic function, with figured-bass notation for its voicing. The same physical stimulus (in this case: a chord surface realisation of C-major) plays, in these two contexts, different harmonic functions as target: dominant (V^3; top) in the key of F major, and tonic (I; bottom) in the key of C major. Bottom of figure: Task structure across the three conditions. The diagonally-hashed background shows the epoch modelled in the GLM, which produced betas for all subsequent fMRI analyses.

Each trial began with a fixation cross presented for 2.5s±0.83s (jittered across trials). The condition-appropriate stimulus was then played back while a count-down timer displayed the number of chords remaining. During both the context and target epochs of the stimuli (i.e., all 7 chords, in **P** and **I**), participants were instructed to *actively* listen, that is, sing along in their minds, silently but subvocalising, irrespective of whether the target was audible (**P**) or muted (**I**). During the subsequent "imagine" task epoch (4s), in all conditions, participants were asked to vividly imagine the target chord in their mind, and prepare humming out loud a corresponding note; which they would do during the subsequent "hum" task epoch (4s). The final task epoch, "rate", displayed a scale on which participants rated the vividness of the foregoing imagery, from 1 to 5, using buttons on an MR-compatible button-box, without a time limit.

The visual display for all epochs generally consisted of a small icon on a 50%-grey background, indicating the current task epoch (see Figure 1). Sounds were presented through MR-compatible headphones, with participants wearing earplugs to protect against scanner noises. To ensure a good SNR between scanner noise and the music, the volume was set at the maximal level that each participant deemed comfortable.

Trials were blocked according to condition, with **P** and **I** blocks consisting of 8 trials (exemplars), and 2 for **C** (see Table 1). Within each block, trials were presented in randomised order. There were 6 blocks per run, i.e. 2 repetitions

of each block type (condition). Each participant thus heard 144 stimuli in total, distributed over four ~14min functional runs (4 runs × 3 conditions × 2 repetitions × 8/8/2 stimuli per **P**/**I**/**C** block).

After the scanning session, participants completed the Bucknell Auditory Imagery Scale (BAIS-V and BAIS-C; Halpern, 2015) and the Goldsmiths Musical Sophistication Index questionnaires (GMSI; Müllensiefen et al., 2014), providing measures of auditory imagery ability and general musical ability, respectively.

2.3.3 MRI acquisition

Scanning was carried out at TU Dresden's Neuroimaging Centre, using a Siemens Magnetom 3T TrioTim scanner with a Siemens 12-channel head coil (Siemens, Erlangen, Germany). T1-weighted images were acquired with a 3D magnetisation-prepared rapid gradient echo sequence (MP-RAGE), with repetition time (TR) = 1.9s, echo time (TE) = 2.26s, field of view (FOV) = 256x224x176 mm^3, phase=100, voxel size=1x1x1 mm^3, inversion time = 0.9s, flip angle (FA) = 9°, phase partial Fourier 7/8, and bandwidth (BW) = 200Hz/Px. For functional imaging, an echo-planar imaging (EPI) sequence was employed, with TR = 2s, TE = 25 ms, FOV = 192x192x136 mm^3, 34 slices, voxel size = 3x3x3.2 mm^3, slice gap 25%, FA = 78°, BW = 2004Hz/Px, AC-PC tilted slices with descending slice order.

2.4. Analysis of the behavioural data

Vividness ratings were submitted to separate linear mixed-effects models (LMEs). Each LME had *Condition*, *Key* and *HarmonicFn* defined as fixed effects, with all main effects and the *Condition* × *HarmonicFn* interaction term defined. Participant identity and stimulus identity (that is, exemplar name, see Table 1) were defined as random effects.

2.5. Analysis of the fMRI data

To be able to track how different aspects of auditory imagery (e.g. its rule-based/memory-based origin; Halpern & Zatorre, 1999) are encoded within different parts of the auditory cortex and its connected structures, we make use of multivariate decoding methods (Varoquaux & Poldrack, 2019), able to link auditory/musical features with activity in *distributed* brain areas. We specifically test our hypotheses using decoding models and RSA. Decoding models inform about the discriminative power of neural activity as a function of the stimuli's category (harmonic function) or modality (perceived or imagined). Conversely, RSA paves the way towards a generative account, by suggesting similarity between theoretical and measured neural representations. For details about the preprocessing of the anatomical and the functional MRI data, see the Supplementary Methods.

2.5.1 Regions of interest

We defined four bilateral regions of interest (ROIs) that we deemed the most relevant given the cited literature. From the ROI version of the MIST Atlas, a multi-resolution parcellation of functional brain networks (Urchs et al., 2019), we identified four bilateral structures, namely those labelled as Heschl's gyrus ("HSgyr"; henceforth HG), which includes 545 voxels for the right ROI and 205 voxels for the left one; the middle part of the superior temporal gyrus (STgyr_m), with 281 voxels for right, 275 for left; the anterior and posterior segments of SMA (respectively PSMCor_a, i.e. pre-SMA; and SMA proper, hereafter SMA), with 312 voxels for right, 360 for left; and PSMCor_p, i.e. SMA proper, with 179 voxels for right, 132 for left. All these ROIs are depicted in Figure 2.

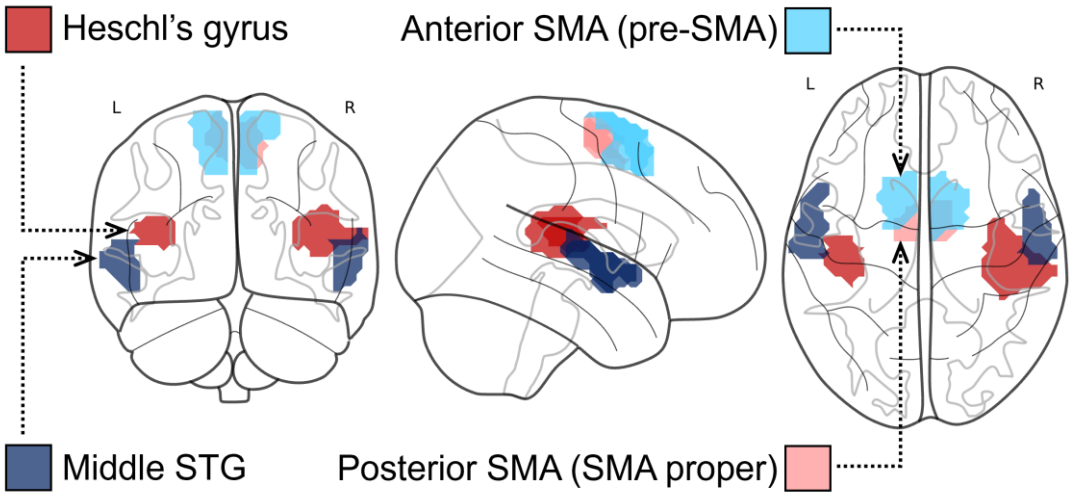

Figure 2: **Regions of interest.** Depiction of the four bilateral ROIs chosen, in coronal, sagittal and axial views. Colours are assigned to ROIs arbitrarily, in glass brain rendering.

2.5.2 Univariate analyses

Nilearn version 0.7.1 was used to estimate whole-brain activation maps. A first-level, subject-wise General Linear Model (GLM) was estimated to model the effect of the 2 × 2 stimulus categories (Tonic/Dominant; and C/F#) and of the two main conditions (**P** and **I**) as eight separate regressors, using the whole-brain, standardised BOLD time series (MNI152NLin2009cAsym, with a voxel size of 3x3x3 mm), as well as the two *Surface* categories (C/F#) for the control condition. For each stimulus presentation, the event of interest was modelled using the onset of the Imagine epoch (see Figure 1), with a duration of 4s (2 TRs). In addition, we also included regressors of no interest corresponding to the main events in the experimental design, such as the chord presentation, the onset of the humming epoch, and the rating epoch. For instance, we modelled the presentation of the seven chords with one long event lasting for 7 TRs irrespective of condition (**P** or **I**), to emphasise that our event of interest lies in the imagine epoch.

We used the SPM hemodynamic response function (as part of the *glm* module of *Nilearn*), with dispersion and derivative, and modelled the drift using the discrete cosine transform outputs of fMRIPrep. Nuisance regressors were loaded from fMRIPrep's outputs using load_confounds (https://github.com/SIMEXP/load_confounds). These included the following time series: motion parameters with derivatives and squared derivatives, drift modelled by discrete cosine transform, white matter and CSF signal, as well as the time series of noisy components estimated by ICA AROMA(Pruim et al., 2015). A single GLM was estimated by modeling all four runs together, and we used the obtained regressors of interest to compute contrasts estimating differences due to harmonic function (Tonic vs. Dominant category) or surface chord (C vs. F# category) of the target chord; and task condition (**P**, **I** or **C**), yielding six first-level statistical maps per subject for **P** and **I** (P: T>D, C>F#; I: T>D, C>F#; P>I; I>P), and one contrast for **C** (C>F#). A second-level, group-wise analysis was estimated subsequently, using one sample t-tests. We report results with a conservative false positive rate (FPR) of $p<0.001$, and results corrected for multiple comparisons using family-wise error rate (FWER) at $p<0.05$) . In all cases, we also corrected for clusters extents larger than 10 voxels.

Additionally, we also specified models where the BAIS and GMSI scores were added as covariates (in addition to the regressors of interests present), for the subset of 19 subjects for which those questionnaire data were available. The same was done for the vividness rating scores.

Identification of anatomical structures in the result clusters was based on the Harvard–Oxford cortical/subcortical structural atlas, as provided in AtlasReader (Notter et al., 2019; https://github.com/miykael/atlasreader).

2.5.3 General Linear Model for multivariate analyses

In order to perform the subsequent multivariate analyses (decoding and RSA; see below) at the single trial level, we also fitted run-wise & subject-wise GLMs, in which each presentation of a stimulus is considered as a separate regressor. As with the univariate analysis, for each stimulus presentation, the event of interest was modelled using the onset of the Imagine epoch, with a duration of 4s (2 TRs). A separate GLM was fitted for each run, using th e brain mask estimated for it by fMRIPrep, and using the same model settings (confounds, and hemodynamic response model) as in the univariate analysis. From the 8 unique stimuli, presented twice per condition in each run, we obtained a total of 32 beta maps per subject per run, all estimated using canonical contrasts of the fitted GLM. Across the four runs, a total of 128 beta maps was obtained, per subject.

2.5.4 Decoding models

We trained decoding models (Varoquaux & Poldrack, 2019) to dissociate brain activity according to sets of experimentally defined labels, thereby using neural signals to distinguish (predict) the associated experimental conditions and stimulus categories. Below, we describe decoding models defined with all subjects' data in voxels from separate ROIs. In the Supplementary Methods, we also present subject-wise analyses performed on the whole-brain, akin to a searchlight, using spatial regularisation and clustering to reduce the number of features.

The inputs (training data) for decoding models were obtained from the subject-wise, run-wise beta maps for each stimulus presentation, by selecting voxels in each ROI separately, after applying a 5 mm FWHM spatial smoothing. As the ROIs comprised relatively large areas, i.e. many classification features in relation to the number of trials, we estimated decoding models using all 35 subjects and all the ROI's voxels at once, thus providing classifiers with reasonable statistical power (4480 total examples, with 160 to 500 voxels per ROI). All de coding models were trained using leave-one-out cross-validation, keeping one run for testing across all subjects; the accuracies we report are averaged across runs. Decoding models were trained using logistic regression with L2 regularisation (penalty of C=1) using the "Decoder" method from *Nilearn* v0.7.1. All voxels in each ROI were used (parameter "screening perce ntile" set to 100%).

Using this setup, for each ROI we estimated the classification accuracy when training decoding models to predict the following labels: two *HarmonicFn* categories in **P** (1a) and in **I** (1b), two *Surface* chords in **P** (2a) and **I** (2b), four *Keys* in **P** (3a) and **I** (3b), eight exemplars in **P** (4a) and **I** (4b), two exemplars (single chords) in **C** (5), and finally **P** and **I** across all stimuli (6). Whenever models were defined using either **P** or **I** (a and b labels above), we also tested a cross-modal setup, in which the model trained on **P** data was tested for its performance on **I**, and vice-versa. In addition, as *HarmonicFn* was of primary interest, we also investigated to what extent decoding mistakes originated there, using contingency matrices that display *HarmonicFn* as ground-truth, and *Key* as predictor (cf Figure 6). For each setting, chance level was estimated using the "dummy" classifier as implemented in the "Decoder" method, which estimates chance level according to the distribution of labels in each class of the training sets (corresponding to the "stratified" strategy in *sklearn*: https://scikit-learn.org/stable/modules/generated/sklearn.dummy.DummyClassifier.html). Estimated chance levels were 48.8% for *Condition*, 50.9% for *HarmonicFn,* 53.0% for *Surface* in **P** and **I** and 50.7% in **C**, 63.5% for *Key* and 77.6% for *Stimulus* (individual exemplars). We report models as significantly "above chance" when the average accuracy is at least one standard deviation above the estimated chance level.

All decoding analyses and associated data preparation steps were done in *Nilearn* v0.7.1.

2.5.5 Representational Similarity Analysis

We use RSA to check which representational geometries arise when brain data map onto chord- and phrase-level harmonic representations (harmonic function and key respectively). Rather than compare brains and models at the level of activity patterns (as with decoding), with RSA we compare representations at the level of representational dissimilarity matrices (RDMs; Kriegeskorte & Kievit, 2013).

RSA is performed in two steps: participant-level estimation of empirical (in our case: fMRI-based neural) RDMs; and group-level estimation of model fit, with theoretical RDMs. Theoretical RDMs are based on stimulus categories and experimental conditions, reflecting our hypotheses. Namely, theoretical RDMs allow a useful characterisation of the representational geometry corresponding to the tonic or dominant targets chosen here to reflect predictive scenarios accruing during a musical cadence.

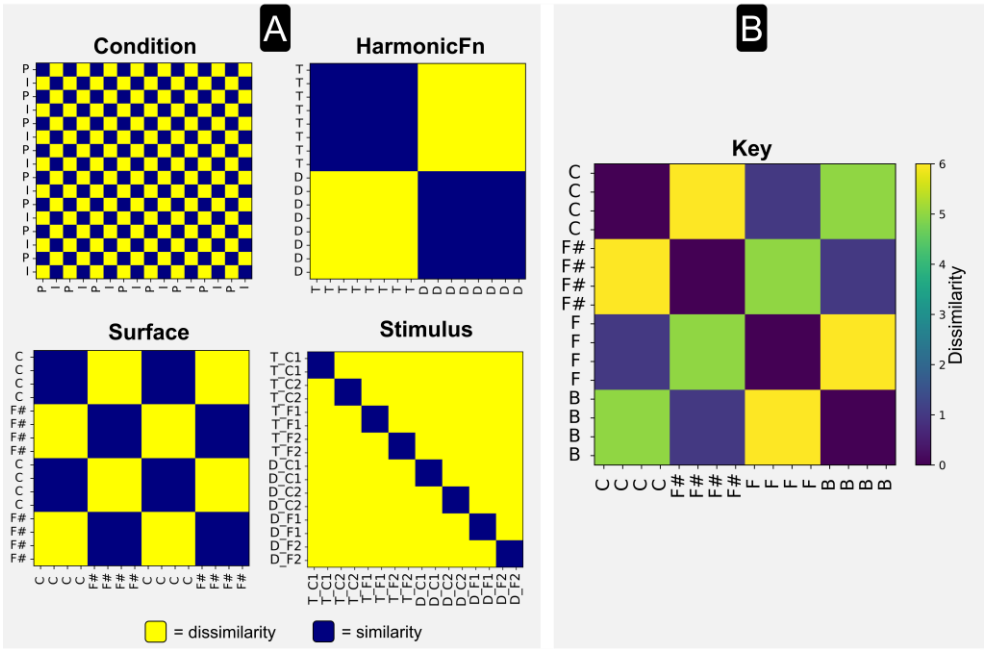

Figure 3: **Representational Similarity Analysis.** Model RDMs (representational dissimilarity matrices) for Condition, HarmonicFn, Surface, Stimulus (panel A) and Key (panel B).

A | Cells represent stimulus pairs: blue indicates their similarity (encoded as 0), and yellow dissimilarity (encoded as 1). The Stimulus RDM namely encodes the repetition of stimuli across P and I (with the exception of the omitted final chord in I), and therefore corresponds to a block diagonal matrix.

B | In the Key RDM, by contrast, the colour encodes step-wise dissimilarity, according to the minimal number of steps between pairs of keys on the circle of fifths.

To estimate neural RDMs, we aimed to maximise the reliability of dissimilarity measures by computing the leave-one-run-out cross-validated Mahalanobis distance ("crossnobis distance") between beta maps, which includes multivariate noise normalisation using GLM residuals (Walther et al., 2016). Neural RDMs were estimated separately

for each ROI, by extracting corresponding voxels before calculating crossnobis distances. Five theoretical RDMs were defined (see Figure 3), according to *Condition* (**P** and **I**); *Surface* (C and F#), *HarmonicFn* (tonic and dominant), *Key* (B, C, F and F# major), and *Stimulus* (eight different exemplars across P and I).

In all cases, RDMs model the stimuli for the whole experiment; each model considers one feature of interest at a time. The *HarmonicFn* RDM models dissimilarity with a binary variable for each stimulus pair corresponding to same or different harmonic function, irrespective of condition, surface, individual stimulus exemplar, or key. The *Key* RDM quantifies dissimilarity using distance between pairs of keys on the circle of fifths (e.g. the keys of C and F are one step apart, while C and F# are five steps apart)[1]. We also defined an additional model for *Stimulus,* corresponding to individual exemplars, coded 0 for similar and 1 for different. Importantly, the *HarmonicFn, Surface, Stimulus* and *Key* RDMs are tested across **P** and **I** pooled together, to uncover a general effect of stimulus property.

Group-level model inference was performed by correlating neural RDMs with theoretical RDMs using cosine similarity between the two as a measure of RDM prediction accuracy. To build a permutation-based null model, the lower and higher bounds of the noise ceiling were estimated using bootstrap resampling of experimental conditions and participants, with 1000 permutations. The higher-bounds of the noise ceiling were above a cosine similarity of 0.2 for all ROIs. The highest higher-bound was 0.3, for right STG; and the lowest lower-bound was 0.02, for left SMA. We used one-sample t-tests to compare each model performance to 0, and test whether models are below the lower-bound estimate of the noise ceiling, with Bonferroni correction for multiple comparisons. In all ROIs, none of the models was significantly below the lower bound of the noise ceiling.

Model comparisons were performed using post-hoc pairwise tests, corrected using the False Discovery Rate (FDR, $p < 0.01$, 6 model-pair comparisons). All RSA model estimations (with statistical tests implemented by model inference functions, detailed in the Supplementary methods), comparisons and visualisations were done using *pyRSA* (https://github.com/rsagroup/pyRSA) and *Nilearn* v0.7.1.

2.6. Data availability

For legal reasons, we are not allowed to publish the raw data (neither MRI nor behavioural). However, there is permission to share the tasks, stimuli, beta maps and analysis scripts; those are all available at https://osf.io/qu5vy/, which links further to NeuroVault and GitHub repositories.

[1] The results are similar if, instead of defining the Key RDM in terms of step-distance on the circle of fifths, a binary approach is used as in the other RDMs (i.e., same or different key).

3. RESULTS

3.1. MI vividness in the presence of a harmonic context

Distributions of vividness ratings are depicted in Figure 4 (for linear model estimations, see Supplementary Table S1). Neither *HarmonicFn* nor *Condition* significantly predicted ratings, likely due to a ceiling effect. The fixed effect of *Key* on ratings was significant, however that is likely to be due simply to the (often quasi-harmonic) scanner noise. This will have necessarily interfered differentially with the stimulus in the P condition. Therefore, this effect will not be discussed further.

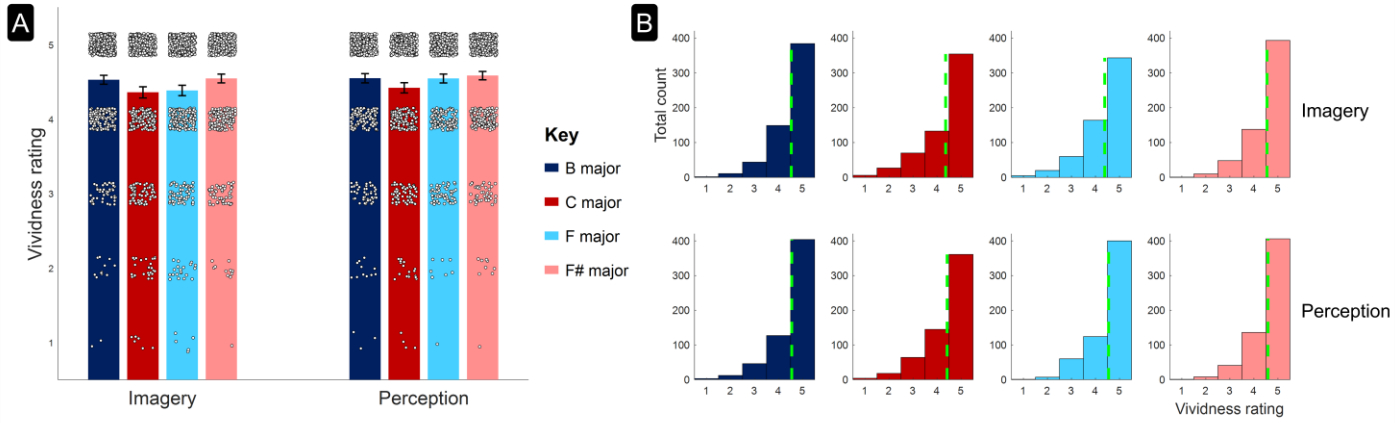

Figure 4: **Behavioural results (vividness ratings)**. Distributions are shown across the Imagery and Perception conditions, further grouped by stimulus *Key*, which was the only significant fixed-effects factor in a linear mixed-effects model.
A | Data points represent individual subject ratings at each trial, and are jittered horizontally & vertically to aid visualisation. Error bars show 95% confidence intervals around means.
B | The same means are marked with a vertical dashed green line, for every distribution.

3.2. Brain activation maps contrasting stimulus categories and task conditions

Estimating whole brain activation maps using the general linear model, we found an overall effect of **P** > **I** (Figure 2A and Table S2), in the bilateral superior temporal gyri, the right occipital fusiform gyrus and left SMA.

In **C** we did not find any effect of target chord in the absence of a preceding context (*Surface*: $p_{FPR} > 0.001$). In **P**, the *Surface* contrast revealed an effect in three small clusters, but no effect of *HarmonicFn*. In **I**, for *Surface* we found two large bilateral clusters in superior temporal gyri and one cluster in left frontal cortex; and for *HarmonicFn*, two clusters in the right STG and medial post-central gyrus (see Figure 2B and Table S2 for peak coordinates and statistics). When defining those second-level contrasts with GMSI or BAIS as regressors, no significant clusters remained ($p_{FPR} > 0.001$).

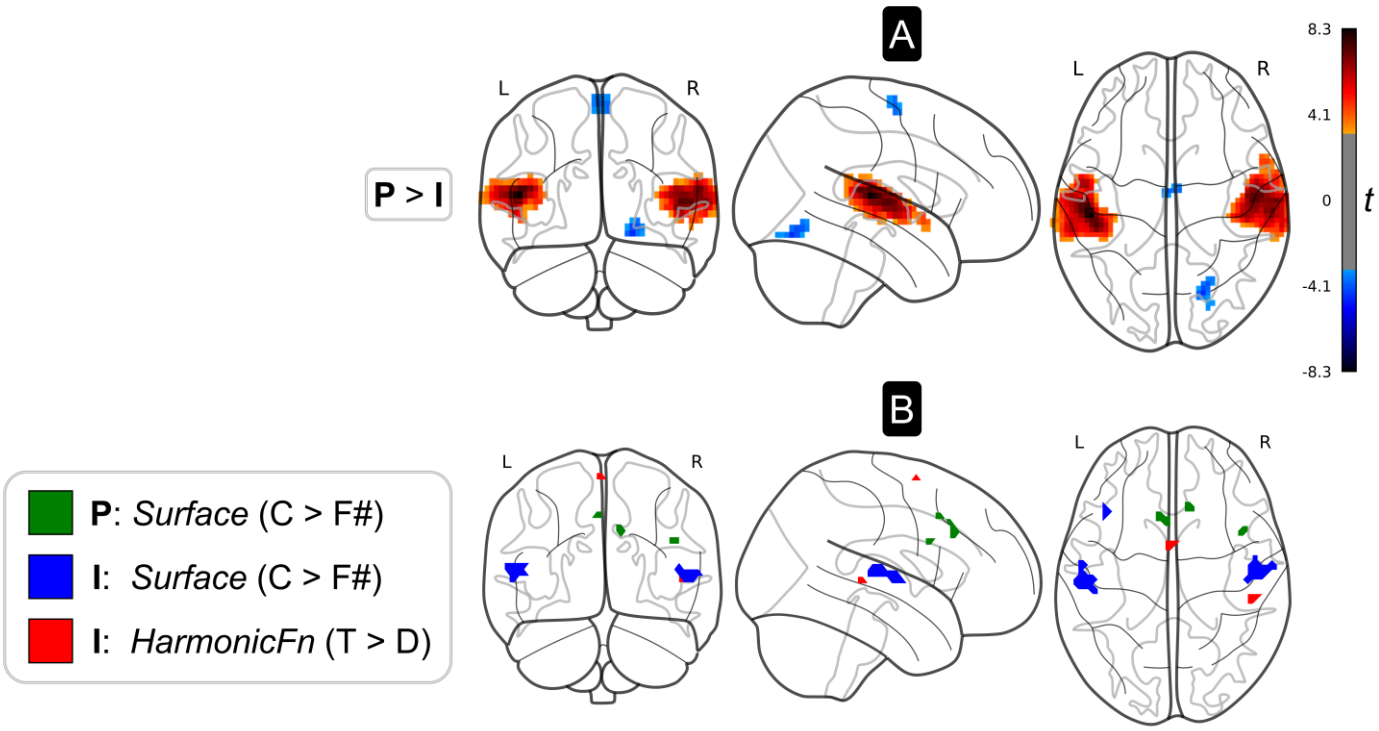

Figure 5: **Whole-brain univariate second-level GLM contrasts** ($p_{FPR} < 0.001$, cluster extent threshold: k = 10 voxels).
A | Thresholded statistical map for the contrast "**P** > **I**", with positive clusters in bilateral superior temporal gyri and small negative clusters in right occipital fusiform gyrus and left SMA. The colour bar indexes values of the *t*-statistic.
B | Significant binarised clusters in: bilateral paracingulate gyrus and right middle frontal gyrus, for contrast "**P** / *Surface* (C > F#)", green-filled contours; in bilateral Heschl's gyrus (HG) and left frontal orbital cortex, for "**I** / *Surface* (C > F#)", blue-filled contours; and in right superior temporal gyrus and left SMA, for "**I** / *HarmonicFn* (T > D)", red-filled contours. For peak values and coordinates, see Table S2.

3.3. Decoding harmonic function and key

We subsequently trained decoding models on single-trial brain activation maps in ROIs (see Methods). First, we were not able to classify *Surface*, in any of the 3 conditions, for any ROI. The same was true for *HarmonicFn* (in both **P** and **I**).

Decoding models for *Condition* had above-chance accuracy in the left STG (53.0±1.4%), right STG (54.0±0.7%), left HG (52.9±0.1%) and right HG (53.7±0.7%). *Stimulus* could be successfully decoded except in the right HG and the left pre-SMA, under both **P** and **I**. For *Key*, models were above chance in left HG and bilateral SMA, in both **P** and **I** (see Table S3).

In Figure 6, we depict the decoding models for *Key* in left SMA and left HG. The contingency matrices show that misclassifications are more likely to occur towards a key where the same rather than a different *HarmonicFn* was employed. That is, predicted keys (matrix columns) occur more often in pairing with the *HarmonicFn* (rows) they were actually associated with, according to the true mapping of our experimental design (see Table 1, which shows how each *Key* corresponds unequivocally to a single *HarmonicFn*). These combinations are represented in Figure 6 by matrix cells with dashed borders.

Recall that our *Key* model was trained to predict *any* of the four keys, from *any* trial. Hence, a proportion of predicted keys will not correspond to the true mapping. However, as the colourmap in Figure 6 suggests, this proportion was on average smaller: in left HG, for **P** (correct, 76.25 occurrences; incorrect, 63.75) and **I** (76.9; 63.1); and left SMA, for **P** (74.75; 64.75) and **I** (73.56; 66.4). Null decoding models estimated using the dummy classifier for *Key* had an opposite pattern (correct, 66.8; incorrect, 73.2). No clear differences between *Key* decoding models could be observed between conditions themselves (**P** vs. **I**).

We also trained whole-brain subject-level decoding models, and had similar results for *Condition*, *Surface*, *Key* and *Stimulus*. Interestingly, such models for *HarmonicFn* yielded slightly above-chance accuracy: 53.7±4.3% in **P** and 54.2±4.6% in **I** (see Table S4).

Finally, all cross-modal decodings (i.e. classifier trained on **P** and tested on **I**) yielded accuracies no higher than chance.

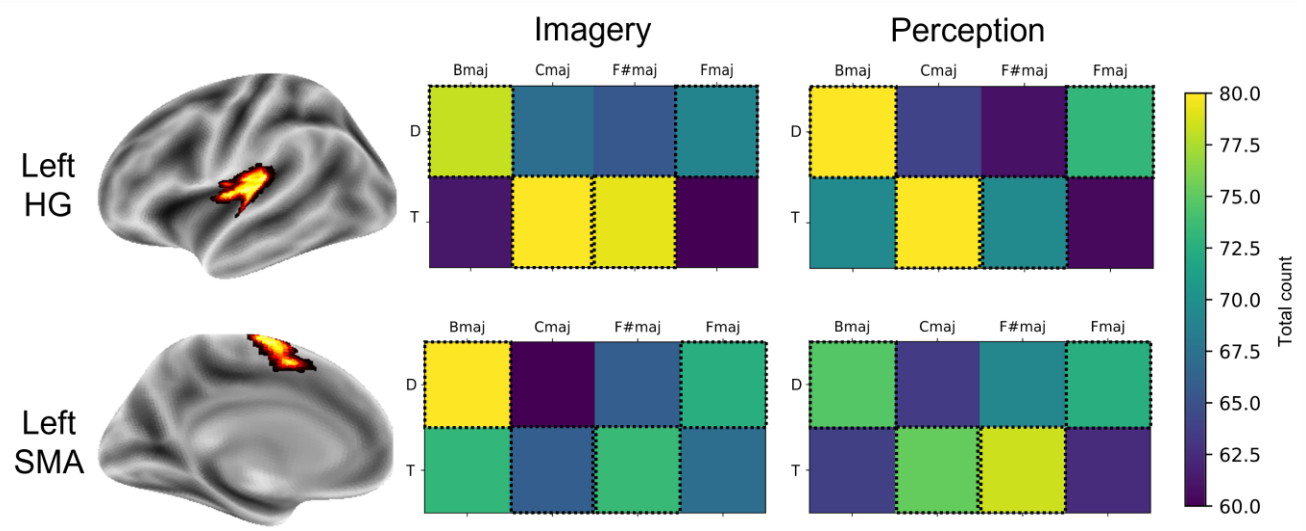

Figure 6: **Decoding results**. Models are shown for *Key*, trained in Imagery (left-hand side matrix) and Perception (right-hand side matrix), from left HG (top row) or left SMA (bottom row). For each of these two ROIs, average logistic regression weights are shown across categories (i.e., *Key*), on an inflated brain. The 2x4 contingency matrices represent predicted *Key* labels (across columns) and possible values of *HarmonicFn* labels (across rows). Matrix cells, colour-coded as shown in the colourmap, index average counts across runs, across all participants. Dashed-contoured matrix cells highlight *Key* × *HarmonicFn* combinations that match the true mapping of our experimental design (as per Table 1).

3.4. Chord- and phrase-level harmonic representations across Perception and Imagery

Models based on Representational Dissimilarity Matrices (RDMs, Figure 3) were defined and tested using fMRI responses in ROIs to investigate neural representations of *Condition*, *HarmonicFn*, *Key, Stimulus* and *Surface*.

For left and right pre-SMA, all models performed above zero. For right SMA, only the *Key* model was above zero, and for left SMA, only the *Condition* model. In bilateral SMA and pre-SMA ROIs, pairwise comparisons between models revealed no significant differences.

For the temporal ROIs (Figure 7A), all RDMs performed above zero in the right HG and left STG. In the left HG, the *Surface* and *Stimulus* model did not perform above zero, and in the right STG, only *Condition* did. The *Condition* model had higher accuracy than *Surface, Key,* and *HarmonicFn* in the left HG, right and left STG, and had higher accuracy than the *Stimulus* model in the right STG. *Key* had higher accuracy than *Surface* in right HG, left HG and left STG. Finally, *Stimulus* had higher accuracy than *Key*, *HarmonicFn* and *Surface* in left STG.

In addition, when bootstrapping across conditions for the same temporal ROIs, pairwise significant differences between models are lost. In the right Heschl's gyrus and left STG, all models perform above zero, while only the *Condition* model still performs better than zero in the left Heschl's gyrus and the right STG (see Figure 7B).

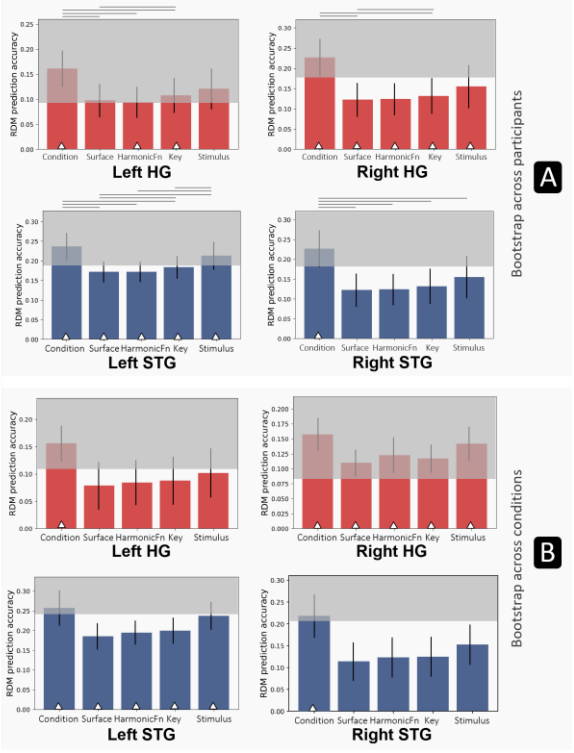

Figure 7: **RSA results**. Bar heights show RDM prediction accuracy (cosine similarity, averaged across subjects) of each of the five models (*Condition, Surface, HarmonicFn, Key, Stimulus*), for temporal-lobe ROIs: bilateral Heschl's gyrus, HG; and bilateral superior temporal gyrus, STG (see also Figure 2). △ at the base of bars indicates the model has >0 accuracy (one-tailed *t*-test, Bonferroni-corrected. Horizontal lines show statistically-significant pairwise differences between models (six model-pair comparisons, FDR corrected $p<0.01$), the most consequential one being *Key>Surface*, for left STG and bilateral HG. Lower and higher bounds of the noise ceiling are indicated by the grey shading.

A | Bounds estimated using bootstrap resampling across participants.

B | Bounds estimated using bootstrap resampling across conditions.

4. DISCUSSION

We investigated MI through the lens of harmonic syntax. We checked whether expectation accruing within canonical chord sequences (authentic- or half-cadences) is salient enough to be retrieved from brain activity elicited while hearing or imagining the sequence's final chord. Whole-brain decoding models differentiated the harmonic function (tonic or dominant) under which those chords were employed. At ROI level (bilateral SMA, left HG), we also could decode the corresponding key of the sequence. Representational Similarity Analyses supported this, by finding that our fMRI data explain the model RDMs defined. Namely, bilateral STG and bilateral HG dissimilarly encoded neural representations between perceived and imagined chords, while left STG and bilateral HG more saliently encoded the sequence's key than the surface realisation of its final chord.

Higher activation in **P** than in **I** was observed in two large bilateral clusters that included HG. Congruently, the *Condition* RDM best explained the data across all ROIs. Recall that our GLM modelled activity during the final ("Imagine") epoch of a trial, silent in both **P** and **I** (Figure 1). Still, the stronger auditory cortex activity in **P** might have been due to a more recent echoic trace from the previous "target" epoch, audible in **P** but not in **I** (Linke & Cusack, 2015). This result, in line with suggestions that different patterns of brain activity are evoked at the onset vs. during sustained MI (Janata, 2001), validates our condition manipulation.

Our decoding results allowed relating the target chord's harmonic function to the sequence's overall key. First, models for *Key* decoding performed best in left SMA, but were still above-chance in most ROIs. The SMA's prominence over e.g. the temporal ROIs may speak to the prominence of subvocalisation in our active listening paradigm for triggering imagery in a harmonic context. The extent to which imagery tasks are consciously experienced varies greatly (Schaefer, 2014), and the SMA might be particularly involved when MI is generated endogenously rather than triggered through external references (Bastepe-Gray et al., 2020). Second, *HarmonicFn* decoding was above-chance with whole-brain subject-level models. This was not the case for ROI group-level models, where *HarmonicFn* was only vicariously decodable, through *Key*. Namely, predicted keys preferentially corresponded to the *HarmonicFn* they were mapped to in our design (see Table 1 and Figure 6). In other words, decoding models for *Key* reassuringly favoured keys sharing the same *HarmonicFn*.

Thus, albeit indirectly, our decoding model still distinguishes between the *HarmonicFn* levels constituting our critical manipulation. Indeed, the decoding literature suggests that stimuli may occasionally be successfully classified only by some secondary dimension with which the primary dimension of interest is intrinsically linked (Chu et al., 2011). Taken together, these results suggest that, while the *HarmonicFn* of the chord ending the sequence cannot be decoded explicitly, the identity of individual exemplars can be – through decoding either of the stimuli themselves (as done elsewhere, e.g. Klein & Zatorre, 2015); or, crucially, of their associated key. For all intents and purposes, this renders Tonic/Dominant as distinguishable categories. The RSA results went on to support this interpretation: while the RDM encoding *Stimulus* had higher prediction accuracy than *Surface*, *Key* and *HarmonicFn* in left STG, *Key* was higher than *Surface* in both left STG and bilateral HG, consistent with these regions' role in the predictive coding hierarchy (Kumar et al., 2011; Lumaca et al., 2020). Overall, this suggests the (global) harmonic feature of a chord sequence's key yields a more salient brain representation than the surface realisation of its closing chord.

That multivariate fMRI can reveal abstracted imagery representations, such as our *Key* RDM vs. *Surface*, had already been suggested by Linke & Cusack (2015) who, from a similar set of ROIs, decoded semantic information of imagined (non-musical) sound along orthogonal categories. This suggested auditory imagery is not confined to veridical representations aspiring towards perception-like vividness, as when rehearsing a sound to oneself, but can draw on abstract long-term knowledge. We suggest our results reflect such an abstraction, but in the realm of harmonic processing. Specifically, that harmonic function, operating along the perception–imagery continuum, acts as a generative model transforming surface representations of chords into internal representations, at time-scales long-enough to be characterised by a musical key. Indeed, our active-listening paradigm affords an increased rate of evidence accumulation (decreasing entropy; Koelsch et al., 2019; Vuust et al., 2022), as listeners are cued about upcoming syntactic events through context chords. These gradually sharpen the mental image of the phrase-closing chord, thereby articulating the current key. Our results therefore also speak to the debate over the veridical vs. abstracted nature of representations in mental imagery (Pylyshyn, 2002, 2003).

A number of other MI studies similarly found evidence of abstracted MI representations. Using EEG decoding, Di Liberto, Marion and colleagues (2021; 2021) concluded that melodic expectation mechanisms are as faithfully encoded during MI as during listening, in that imagery responses are effectively top-down predictive signals set against bottom-up sensory activations (Koster-Hale & Saxe, 2013). Similarly, Endestad et al. (2020) suggested that the mental effort of imagining or listening a melody unfolds across similar temporal trajectories. Finally, Regev et al.

(2021) found that BOLD patterns recorded from the middle right STG during listening were reactivated during MI in a stimulus-specific manner, and are thus specific to the imagined content. Differently to ours, these studies used unharmonised melodic stimuli, and asked participants to refrain from (sub)vocalising, thereby tapping into qualitatively-different mechanisms of MI generation. Nonetheless, a unifying perspective emerges from this body of work, whereby endogenous auditory predictions support a generative melodic engine, active during both listening and imagery. Our results complete this perspective, pointing to temporal and premotor regions capable to, additionally, also encode harmonic expectation.

The way a familiar musical piece is re-created through imagined expectation has also been described phenomenologically. Using elicitation interviews, Huovinen & Tuuri (2019) outline the music-structural tendencies in participants' self-reported experiences, for instance how certain sections of inner listening are accompanied by feelings of expectancy of forthcoming musical events. By guiding listeners' expectations along canonical cadences, we approached MI as an "expectant" and voluntary mental action (Janata, 2001). Our decoding results suggest that the activity in left SMA & superior temporal cortices may be involved in the process underlying the base imagery mechanism; while our encoding models (RSA) suggest that superior temporal cortices sustain neural representations of a putative modality-independent generative model of harmonic function.

The difference between our **P** and **I** conditions lay in the 2s target-chord epoch (Figure 1). Therefore, our critical manipulation of *HarmonicFn* within that epoch might have been too subtle for Tonic and Dominant endings to produce distinguishable patterns of brain activity. That this manipulation, expressed vicariously through *Key*, was nonetheless decodable and (in RSA) representationally-distinct reassures our conclusions. Future research can build on this proof of concept to better characterise the formation of expectations within chord progressions playing out in one's mind. Inter-individual differences are bound to modulate this. Unfortunately, for no part of the fMRI analyses could we – with sufficient statistical power – link our harmonic manipulation to general and imagery-related musical abilities, as the GMSI and BAIS questionnaire data were only available for a subset of our sample.

Insofar as our study described – at the neural level – a microcosm of the unfolding of imagined harmonic expectations, it will be interesting if future work extended this description to the phenomenon's natural scale: *entire* musical pieces imagined voluntarily. Ingenious paradigms providing objective trial-by-trial measures of imagery's accuracy *and* vividness (Gelding et al., 2015) can profitably connect with qualitative insights such as Huovinen & Tuuri's (2019) phenomenological taxonomy of MI. This can yield hypotheses, e.g. about how M is initiated and maintained, that neuroimaging can test by examining how sections of a piece are qualitatively transformed during inner listening. Better understanding how we wilfully create and guide the experience of tonal music in our minds would attain a replete description of MI as an engine for inner creation of music, whether recreationally or creatively as a compositional tool.

Our results provide tentative support for the existence of an extended network that encodes stimulus dimensions reflecting an internalisation of abstract concepts such as key. These operate during imagery as they do during perception, and indeed along the subvocalisation-afforded continuum between them. The specifics of how, from this network, a generative cognition emerges that more widely supports music's listening and imagery are to be discovered by further research.

5. REFERENCES

Bangert, M., Peschel, T., Schlaug, G., Rotte, M., Drescher, D., Hinrichs, H., Heinze, H.-J., & Altenmüller, E. (2006). Shared networks for auditory and motor processing in professional pianists: Evidence from fMRI conjunction. *Neuroimage*, *30*(3), 917–926.

Bastepe-Gray, S. E., Acer, N., Gumus, K. Z., Gray, J. F., & Degirmencioglu, L. (2020). Not all imagery is created equal: A functional Magnetic resonance imaging study of internally driven and symbol driven musical performance imagery. *Journal of Chemical Neuroanatomy*, *104*, 101748. https://doi.org/10.1016/j.jchemneu.2020.101748

Bastos, A. M., Usrey, W. M., Adams, R. A., Mangun, G. R., Fries, P., & Friston, K. J. (2012). Canonical microcircuits for predictive coding. *Neuron*, *76*(4), 695–711.

Chu, C., Ni, Y., Tan, G., Saunders, C. J., & Ashburner, J. (2011). Kernel regression for fMRI pattern prediction. *NeuroImage*, *56*(2), 662–673.

Clark, A. (2013). Whatever next? Predictive brains, situated agents, and the future of cognitive science. *Behavioral and Brain Sciences*, *36*(3), 181–204. https://doi.org/10.1017/S0140525X12000477

Di Liberto, G. M., Marion, G., & Shamma, S. A. (2021). The music of silence. Part II: Music Listening Induces Imagery Responses. *The Journal of Neuroscience*, JN-RM-0184-21. https://doi.org/10.1523/JNEUROSCI.0184-21.2021

Endestad, T., Godøy, R. I., Sneve, M. H., Hagen, T., Bochynska, A., & Laeng, B. (2020). Mental Effort When Playing, Listening, and Imagining Music in One Pianist's Eyes and Brain. *Frontiers in Human Neuroscience*, *14*, 576888. https://doi.org/10.3389/fnhum.2020.576888

Farbood, M. M. (2012). A Parametric, Temporal Model of Musical Tension. *Music Perception: An Interdisciplinary Journal*, *29*(4), 387–428. https://doi.org/10.1525/mp.2012.29.4.387

Farrugia, N., Jakubowski, K., Cusack, R., & Stewart, L. (2015). Tunes stuck in your brain: The frequency and affective evaluation of involuntary musical imagery correlate with cortical structure. *Consciousness and Cognition*, *35*, 66–77. https://doi.org/10.1016/j.concog.2015.04.020

Friston, K., Mattout, J., & Kilner, J. (2011). Action understanding and active inference. *Biological Cybernetics*, *104*(1), 137–160. https://doi.org/10.1007/s00422-011-0424-z

Gauldin, R. (2000). *Harmonic Practice in Tonal Music*. W. W. Norton, Incorporated.

Gelding, R. W., Thompson, W. F., & Johnson, B. W. (2015). The Pitch Imagery Arrow Task: Effects of Musical Training, Vividness, and Mental Control. *PLoS ONE*, *10*(3), e0121809. https://doi.org/10.1371/journal.pone.0121809

Gordon, E. (1984). A Longitudinal Predictive Validity Study of the Intermediate Measures of Music Audiation. *Bulletin of the Council for Research in Music Education*, *78*, 1–23.

Gracyk, T. (2019). Imaginative listening to music. *The Oxford Handbook of Sound and Imagination*, *2*, 467.

Halpern, A. R. (2015). Differences in auditory imagery self-report predict neural and behavioral outcomes. *Psychomusicology: Music, Mind, and Brain*, *25*(1), 37–47. https://doi.org/10.1037/pmu0000081

Halpern, A. R., & Zatorre, R. J. (1999). When That Tune Runs Through Your Head: A PET Investigation of Auditory Imagery for Familiar Melodies. *Cerebral Cortex*, *9*(7), 697–704. https://doi.org/10.1093/cercor/9.7.697

Halpern, A. R., Zatorre, R. J., Bouffard, M., & Johnson, J. A. (2004). Behavioral and neural correlates of perceived and imagined musical timbre. *Neuropsychologia*, *42*(9), 1281–1292. https://doi.org/10.1016/j.neuropsychologia.2003.12.017

Herholz, S. C., Halpern, A. R., & Zatorre, R. J. (2012). Neuronal Correlates of Perception, Imagery, and Memory for Familiar Tunes. *Journal of Cognitive Neuroscience*, *24*(6), 1382–1397. https://doi.org/10.1162/jocn_a_00216

Huovinen, E., & Tuuri, K. (2019). Pleasant Musical Imagery Eliciting Cherished Music in the Second Person. *Music Perception*, *36*(3), 314–330. https://doi.org/10.1525/mp.2019.36.3.314

Huron, D. B. (2006). *Sweet anticipation: Music and the psychology of expectation*. The MIT Press.

Hyer, B. (2001). Tonality. In S. Sadie & J. Tyrrell (Eds.), *The New Grove Dictionary of Music and Musicians* (Vol. 1, pp. 583–594). Oxford University Press. https://doi.org/10.1093/gmo/9781561592630.article.28102

Janata, P. (2001). Neurophysiological Mechanisms Underlying Auditory Image Formation in Music. In R. I. Godøy & H. Jørgensen (Eds.), *Musical Imagery* (pp. 27–47). Lisse: Swets & Zeitlinger.

Kleber, B. A., & Zarate, J. M. (2014). *The neuroscience of singing*. Oxford University Press Oxford, UK.

Klein, M. E., & Zatorre, R. J. (2015). Representations of Invariant Musical Categories Are Decodable by Pattern Analysis of Locally Distributed BOLD Responses in Superior Temporal and Intraparietal Sulci. *Cerebral Cortex*, *25*(7), 1947–1957. https://doi.org/10.1093/cercor/bhu003

Koelsch, S., Vuust, P., & Friston, K. (2019). Predictive Processes and the Peculiar Case of Music. *Trends in Cognitive Sciences*, *23*(1), 63–77. https://doi.org/10.1016/j.tics.2018.10.006

Koster-Hale, J., & Saxe, R. (2013). Theory of mind: A neural prediction problem. *Neuron*, *79*(5), 836–848.

Kraemer, D. J. M., Macrae, C. N., Green, A. E., & Kelley, W. M. (2005). Musical imagery: Sound of silence activates auditory cortex. *Nature*, *434*(7030), 158–158. https://doi.org/10.1038/434158a

Kriegeskorte, N., & Kievit, R. A. (2013). Representational geometry: Integrating cognition, computation, and the brain. *Trends in Cognitive Sciences*, *17*(8), 401–412. https://doi.org/10.1016/j.tics.2013.06.007

Kumar, S., Sedley, W., Nourski, K. V., Kawasaki, H., Oya, H., Patterson, R. D., Howard, M. A., III, Friston, K. J., & Griffiths, T. D. (2011). Predictive Coding and Pitch Processing in the Auditory Cortex. *Journal of Cognitive Neuroscience*, *23*(10), 3084–3094. https://doi.org/10.1162/jocn_a_00021

Lerdahl, F., & Krumhansl, C. L. (2007). Modeling Tonal Tension. *Music Perception: An Interdisciplinary Journal*, *24*(4), 329–366. https://doi.org/10.1525/mp.2007.24.4.329

Liikkanen, L. A., & Jakubowski, K. (2020). Involuntary musical imagery as a component of ordinary music cognition: A review of empirical evidence. *Psychonomic Bulletin & Review*. https://doi.org/10.3758/s13423-020-01750-7

Lima, C. F., Krishnan, S., & Scott, S. K. (2016). Roles of Supplementary Motor Areas in Auditory Processing and Auditory Imagery. *Trends in Neurosciences*, *39*(8), 527–542. https://doi.org/10.1016/j.tins.2016.06.003

Linke, A. C., & Cusack, R. (2015). Flexible Information Coding in Human Auditory Cortex during Perception, Imagery, and STM of Complex Sounds. *Journal of Cognitive Neuroscience*, *27*(7), 1322–1333. https://doi.org/10.1162/jocn_a_00780

Lumaca, M., Dietz, M. J., Hansen, N. C., Quiroga-Martinez, D. R., & Vuust, P. (2020). Perceptual learning of tone patterns changes the effective connectivity between Heschl's gyrus and planum temporale. *Human Brain Mapping*, *n/a*(n/a). https://doi.org/10.1002/hbm.25269

Marion, G., Di Liberto, G. M., & Shamma, S. A. (2021). The Music of Silence. Part I: Responses to Musical Imagery Encode Melodic Expectations and Acoustics. *The Journal of Neuroscience*, JN-RM-0183-21. https://doi.org/10.1523/JNEUROSCI.0183-21.2021

May, L., Halpern, A. R., Paulsen, S. D., & Casey, M. A. (2022). Imagined Musical Scale Relationships Decoded from Auditory Cortex. *Journal of Cognitive Neuroscience*, *34*(8), 1326–1339. https://doi.org/10.1162/jocn_a_01858

Meyer, K., Kaplan, J. T., Essex, R., Webber, C., Damasio, H., & Damasio, A. (2010). Predicting visual stimuli on the basis of activity in auditory cortices. *Nature Neuroscience*, *13*(6), 667–668. https://doi.org/10.1038/nn.2533

Müllensiefen, D., Gingras, B., Musil, J., & Stewart, L. (2014). The Musicality of Non-Musicians: An Index for Assessing Musical Sophistication in the General Population. *PLoS ONE*, *9*(2), e89642. https://doi.org/10.1371/journal.pone.0089642

Mumford, D. (1992). On the computational architecture of the neocortex: II. The role of cortico-cortical loops. *Biological Cybernetics*, *66*(3), 241–251. https://doi.org/10.1007/BF00198477

Notter, M., Gale, D., Herholz, P., Markello, R., Notter-Bielser, M.-L., & Whitaker, K. (2019). AtlasReader: A Python package to generate coordinate tables, region labels, and informative figures from statistical MRI images. *Journal of Open Source Software*, *4*(34), 1257. https://doi.org/10.21105/joss.01257

Pruim, R. H. R., Mennes, M., Rooij, D., Llera, A., Buitelaar, J. K., & Beckmann, C. F. (2015). ICA-AROMA: A Robust ICA-Based Strategy for Removing Motion Artifacts from fMRI Data. *NeuroImage*, *112*(Supplement C), 267–277. https://doi.org/10.1016/j.neuroimage.2015.02.064.

Pylyshyn, Z. W. (2002). Mental imagery: In search of a theory. *Behavioral and Brain Sciences*, *25*(2), 157–182.

Pylyshyn, Z. W. (2003). Return of the mental image: Are there really pictures in the brain? *Trends in Cognitive Sciences*, *7*(3), 113–118.

Rauschecker, J. P. (2011). An expanded role for the dorsal auditory pathway in sensorimotor control and integration. *Hearing Research*, *271*(1), 16–25. https://doi.org/10.1016/j.heares.2010.09.001

Regev, M., Halpern, A. R., Owen, A. M., Patel, A. D., & Zatorre, R. J. (2021). Mapping Specific Mental Content during Musical Imagery. *Cerebral Cortex*, *bhab036*. https://doi.org/10.1093/cercor/bhab036

Rohrmeier, M. (2013). Musical Expectancy: Bridging Music Theory, Cognitive and Computational Approaches. *Journal of the German-Speaking Society of Music Theory*, *10*(2), 343–371. https://doi.org/10.31751/724

Rohrmeier, M. (2020). The Syntax of Jazz Harmony: Diatonic Tonality, Phrase Structure, and Form. *Music Theory and Analysis (MTA)*, *7*(1), 1–63. https://doi.org/10.11116/MTA.7.1.1

Rohrmeier, M., & Koelsch, S. (2012). Predictive information processing in music cognition. A critical review. *International Journal of Psychophysiology*, *83*(2), 164–175. https://doi.org/10.1016/j.ijpsycho.2011.12.010

Rohrmeier, M., & Neuwirth, M. (2015). Towards a syntax of the classical cadence. In M. Neuwirth & P. Bergé (Eds.), *What is a cadence? Theoretical and Analytical Perspectives on Cadences in the Classical Repertoire* (pp. 287–338). Leuven University Press.

Rohrmeier, M., & Rebuschat, P. (2012). Implicit Learning and Acquisition of Music. *Topics in Cognitive Science*, *4*(4), 525–553. https://doi.org/10.1111/j.1756-8765.2012.01223.x

Sankaran, N., Carlson, T. A., & Thompson, W. F. (2020). The rapid emergence of musical pitch structure in human cortex. *Journal of Neuroscience*. https://doi.org/10.1523/JNEUROSCI.1399-19.2020

Sankaran, N., Thompson, W. F., Carlile, S., & Carlson, T. A. (2018). Decoding the dynamic representation of musical pitch from human brain activity. *Scientific Reports*, *8*(1), Article 1. https://doi.org/10.1038/s41598-018-19222-3

Schaefer, R. S. (2014). Mental Representations in Musical Processing and their Role in Action-Perception Loops. *Empirical Musicology Review*, *9*(3–4), 161–176.

Schürmann, M., Raij, T., Fujiki, N., & Hari, R. (2002). Mind's Ear in a Musician: Where and When in the Brain. *NeuroImage*, *16*(2), 434–440. https://doi.org/10.1006/nimg.2002.1098

Sears, D., Caplin, W. E., & McAdams, S. (2014). Perceiving the Classical Cadence. *Music Perception: An Interdisciplinary Journal*, *31*(5), 397–417. https://doi.org/10.1525/mp.2014.31.5.397

Steedman, M. J. (1984). A generative grammar for jazz chord sequences. *Music Perception*, *2*(1), 52–77.

Tian, X., & Poeppel, D. (2010). Mental imagery of speech and movement implicates the dynamics of internal forward models. *Frontiers in Psychology*, *1*. https://doi.org/10.3389/fpsyg.2010.00166

Tian, X., & Poeppel, D. (2012). Mental imagery of speech: Linking motor and perceptual systems through internal simulation and estimation. *Frontiers in Human Neuroscience*, *6*, 314.

Tillmann, B. (2005). Implicit Investigations of Tonal Knowledge in Nonmusician Listeners. *Annals of the New York Academy of Sciences*, 100–110.

Urchs, S., J, A., C, M., Y, B., J, S.-A., P, O., & P, B. (2019). *MIST: A multi-resolution parcellation of functional brain networks*. https://doi.org/10.12688/mniopenres.12767.2

Varoquaux, G., & Poldrack, R. A. (2019). Predictive models avoid excessive reductionism in cognitive neuroimaging. *Current Opinion in Neurobiology*, *55*, 1–6. https://doi.org/10.1016/j.conb.2018.11.002

Vuust, P., Heggli, O. A., Friston, K. J., & Kringelbach, M. L. (2022). Music in the brain. *Nature Reviews Neuroscience*, 1–19.

Walther, A., Nili, H., Ejaz, N., Alink, A., Kriegeskorte, N., & Diedrichsen, J. (2016). Reliability of dissimilarity measures for multi-voxel pattern analysis. *NeuroImage*, *137*, 188–200. https://doi.org/10.1016/j.neuroimage.2015.12.012

Zatorre, R. J., & Halpern, A. R. (2005). Mental Concerts: Musical Imagery and Auditory Cortex. *Neuron*, *47*(1), 9–12. https://doi.org/10.1016/j.neuron.2005.06.013

Zatorre, R. J., Halpern, A. R., Perry, D. W., Meyer, E., & Evans, A. C. (1996). Hearing in the Mind's Ear: A PET Investigation of Musical Imagery and Perception. *Journal of Cognitive Neuroscience*, *8*(1), 29–46. https://doi.org/10.1162/jocn.1996.8.1.29

6. Acknowledgements

We thank Jonathan Walther, Fabian Moss and Daniel Harasim for engaging discussions in the early stages of the study; Michael Marxen for help with the MR sequences and design, as well as for providing helpful feedback; Katharina Pitt and Elisabete Coelho for help with data collection; Katharina Zwasta for assistance with Matlab processing scripts; Peer Herholz for help with converting the data to BIDS and advice on *fMRIPrep* and *pyRSA*; and Laetitia Saccomani for helpful feedback. Many thanks to Stefan Koelsch for insightful comments on an earlier version of the manuscript.

7. Funding

Part of this research has been conducted under the funding of the Zukunftskonzept (ZUK 64) at Technische Universität Dresden, funded by the Exzellenzinitiative of the Deutsche Forschungsgemeinschaft. Support for TP was provided by a STARS Starting Grant from the University of Padova, and previously by a Marie-Curie Seal of Excellence grant from the University of Trento. MR acknowledges the support of Claude Latour through the Latour Chair in Digital Musicology at EPFL. Contributions to this project have been performed under funding from the European Research Council (ERC) under the European Union's Horizon 2020 research and innovation program under grant agreement No 760081 – PMSB.

8. Author contributions

T.P.: conceptualisation, methodology, task programming, data collection, data analyses, data curation, figures/visualisation, project administration, writing – original draft, writing – review & editing

N.F.: methodology, data analyses, data curation, writing – original draft, writing – review & editing

H.R.: methodology, data collection

O.B.: composition of stimuli

F.B.: conceptualisation, methodology

X.T.: conceptualisation, writing – review & editing

M.R.: conceptualisation, funding acquisition, writing – review & editing

9. Competing interests

The authors declare no competing interests.